Tuning the quantum chemical properties of flavins via modification at C8

Rajiv K. Kar,[†] Sam Chasen,[⁋] Maria-Andrea Mroginski,[†*] Anne-Frances Miller [† ⁋ *]

† Faculty II-Mathematics and Natural Sciences, Technische Universität Berlin, Sekr. PC 14, Strasse des 17. Juni 135, D-10623 Berlin, Germany

⁋ Department of Chemistry, University of Kentucky, Lexington, Kentucky, USA.

** Email: andrea.mroginski@tu-berlin.de and afmill3r2@gmail.com*

KEYWORDS: Flavin, Hammett Constant, Quantum Mechanics, Charge-Transfer, Bond-Length Alternation

ABSTRACT: Flavins are central to countless enzymes, but display different reactivities depending on their environments. This is understood to reflect modulation of the flavin electronic structure. To understand changes in orbital natures, energies and correlation over the ring system, we begin by comparing seven flavin variants differing at C8, exploiting their different electronic spectra to validate quantum chemical calculations. Ground state calculations replicate a Hammett trend and reveal the significance of the flavin π-system. Comparison of higher-level theories establishes CC2 and ACD(2) as methods of choice for characterization of electronic transitions. Charge transfer character and electron correlation prove responsive to the identity of the substituent at C8. Indeed, bond length alternation analysis demonstrates extensive conjugation and delocalization from the C8 position throughout the ring system. Moreover, we succeed in replicating a particularly challenging UV/Vis spectrum by implementing hybrid QM/MM in explicit solvent. Our calculations reveal that presence of non-bonding lone pairs correlates with the change in the UV-vis spectrum observed when the 8-methyl is replaced by NH_2, OH or SH. Thus our computations offer routes to understanding the spectra of flavins with different modifications. This is a first step towards understanding how the same is accomplished by different binding environments.

1. Introduction

Flavins are present in over 100 different enzymes, usually in the form of either flavin mononucleothide (FMN) or flavin adenine dinucleotide (FAD), but covalently modified in some 10% of cases.[1,2] Flavins are at the catalytic or conformational core of dehydrogenases,[3,4] oxidases,[5,6] oxygenases,[7] electron carriers,[8,9] hydrolases,[10–12] light-responsive sensors,[13–15] light-driven DNA repair,[16,17] fuel-producing decarboxylases,[18] dehalogenases,[19] and even magnetosensory navigational systems.[20] Given the extreme versatility of flavins, the second marvel is how individual proteins manage to emphasize a specific activity. Thus, a pervasive goal in the study of flavoenzymes is to understand how the protein environment tunes the flavin electronic structure to favor certain aspects of its reactivity.[21] This is enabled in part by the same virtuosity as is responsible for the enormous repertoire: the molecular orbitals of the redox-active isoalloxazine ring system are extensively delocalized, highly correlated, include positions that are engaged in hydrogen bond donation or acceptance, and even outright acid/base dissociation. Several of the flavin's five physiologically relevant redox and protonation states also have charge. These different states are additionally distinguished by different susceptibilities to geometric distortion.[22,23] Crucially, all of the above can modulate the electronic structure of the flavin. This was at the heart of Massey and Hemmerich's proposal that enzyme sites with different activities favor different electron delocalization within the flavin ring system.[21]

Over the last several years, computation has yielded insights into the distinct reactivities of flavins in several different protein sites, relating their reactivities to their electronic structures.[24–26] To elucidate general principles explaining how the electronic structure of the flavin can be tuned by the protein environment, it is useful to begin with the effects of covalent modifications. First, covalent modification can be expected to produce alterations analogous to those produced in protein active sites. However, the greater strength of covalent bonds can produce larger effects that are easier to detect. Second, the calculations can employ a single well-defined structure rather than the Boltzmann-weighted ensembles that characterize non-covalent interactions. Finally, this approach builds on experimental information already present on different derivatives of the biologically common flavin.

Many flavins have been found covalently attached to amino acid side chains, as reviewed by Scrutton and Fraaije.[3] Besides these, at the C8 position alone, replacements of the methyl with Cl, Br, F, COH, CN, OH, SH and more have been reported.[27–30] Some of these occur in nature .[8,31,32] Many have valuable spectroscopic properties and therefore have been intentionally incorporated in enzymes[4–11]. The reported chemical biology uses them as spectroscopic probes to shed light on the reactivities produced by the protein site.[12–15] However, to understand what their shifts in absorption maxima or reactivities mean, at a fundamental and unifying level, we need to understand the electronic structure that underlies them. Conversely, the electronic spectra employed in experiments also provide invaluable

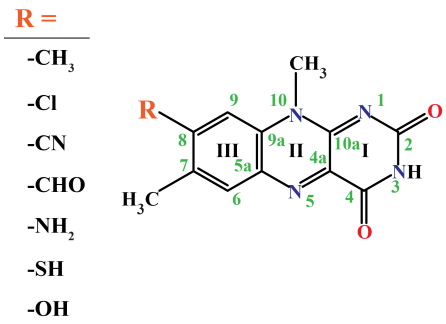

Scheme 1: Chemical structures of lumiflavin with atomic positions numbered in green. 'R' group represents the C8 substituents studied in this work. The uracil ring is shown on the left (ring I), and the xylene ring on the right (ring III). The central ring is the diazabenzene ring (ring II), and the redox-active diazabutadiene system comprises N1, C10a, C4a and N5.

opportunities to test the fidelity of the description provided by computation. This is critical if the computations are to be reliable. Moreover, identification of accurate methods of calculating vertical excitation energy, and thereby optical spectra, remains one of the more challenging aspects of computational chemistry, because the methods need to accurately describe both the ground state (GS) and low-lying excited states as well. Recent successes have been comprehensively reviewed.[33]

The objective of this work is to provide a detailed analysis of how flavin electronic structure responds to different substituents at the C8 position. The dataset comprises seven lumiflavin variants, including the parent molecule with methyl at that position (LF), and variants where methyl is replaced by chloro-, cyano-, formyl-, amino-, mercapto-, or hydroxyl- (Scheme 1). We employ wavefunction and density functional theory (DFT) based methods to study the natures of the first ten electronic transitions. To validate our calculated excitation energies, we compare them with the experimental UV/Vis absorption spectra. Thus, we can improve understanding of how the C8 position tunes the electronic structure and absorption spectra of flavins. Comparison of these methods further enabled us to estimate the theoretical errors in calculated energies and to identify the more suitable quantum chemical method. For a particularly challenging case, we demonstrate the significant improvement obtainable via the use of explicit solvent.

This work is organized as follows: The methodological considerations for geometry optimization, excitation energy calculation with CC2, ADC(2), and wavefunction analysis are explained in section 2, Computational methods. A correlation with Hammett constants, comparison of simulated absorbance spectra with experiments, tabulation of solvatochromic shift, and analyses of charge transfer (CT) are presented in section 3, Results. Finally, we compare the performance of wavefunction-based method with TD-DFT and present an improved method of simulating the absorbance spectra by combining QM/MM sampling and ADC(2). The Discussion closes with emergent insights into flavin reactivity (section 4) and the concluding remarks also note the relevance of this work for deployment of flavins in devices and materials, in section 5.

2. Computational Methods

2.1 Quantum Chemical Calculations

To focus on the flavin itself, the biological ribityl phosphate of FMN and analogous chain of FAD are replaced in our calculations by a methyl group, and the flavin is thus lumiflavin (LF, Scheme 1). Geometry optimization was performed for the ground (S_0) and first excited state (S_1) of LF and the analogs bearing substituents (R) at the C8 position. The optimizations were carried out using B3LYP/6-311++G(d,p), in the gas phase as well as implicit solvent via the conductor-like polarizable continuum (CPCM) model.[34] Bond lengths and dipole moments were extracted from the resulting structures, and atomic charges were calculated using natural bond orbital (NBO) analysis. These calculations were performed using Gaussian *v16*.[35] Values used for Figure 1 were obtained from gas phase calculations and standard deviations were calculated in Excel using STDEV.P. Changes in bond lengths were calculated as GS minus ES (S_0 - S_1) and compared with the corresponding values for the reference LF.

Excitation energies were also calculated for ten low-lying excited states using two popular wavefunction-based methods, correlated second order perturbative method, Coupled Cluster (CC2)[36] and Algebraic Diagrammatic Construction (ADC(2))[36] for comparison with the industry-standard TD-DFT[37] with hybrid functional B3LYP[38] or its range-separated variant CAM-B3LYP[39]. The resolution of identity approximation[40] (RI-CC2 and RI-ADC(2)) was used. Calculations were performed both in gas phase and implicit water (COSMO model)[34] to test for a trend in solvatochromic shifts. CC2 was used to obtain the frontier molecular orbitals involved in electronic transitions (counter value ±0.025). Furthermore, the same method was used to identify the charge-transfer (CT) states based on computed electron density difference plots. The COSMO-RI-CC2 and COSMO-RI-ADC(2) used for calculation of excitation energies is a post-SCF reaction field scheme that is used for coupling between the effect of environment and QM region. The scheme is computationally efficient to that of gas-phase RI-CC2 and RI-ADC(2) calculation, while being able to capture the solvent effect on the excitation energies at linear response level of correlated wavefunction.[41] Representation of molecular orbitals and electron density differences are rendered using Chimera program, using isovalue of ±0.025 [42]

Quantitatve analysis of CT including electron-hole correlation analysis was performed using the plot_OmFrag.py script of TheoDORE program.[43] Wavefunction based methods were performed using the def2-TZVP basis set and their auxiliary basis set using Turbomole *v7.3*.[44] Additionally, the CT analysis for spatial extent associated with electronic transitions – D_{CT}, was also performed for TD-DFT approaches.[45] The calculated vertical excitation energies were convoluted with a Gaussian function to simulate the absorbance spectra, incorporating a broadening of 0.15 eV (full width at half maximum). Experimental spectra are extracted from literature using Webplotdigitizer server.[46]

2.2. Hybrid QM/MM sampling

QM/MM sampling was performed for the amino variant (R=NH_2) using an aqueous solvent box with edges set 9 Å beyond the atoms of the flavin variant. The QM region consisted of the subject molecule comprised of 30 atoms, whereas the solvent molecules (TIP3P water model) were described using MM.[47] Correction for dispersion was included using the D3 variant.[48] The QM region was described with TD-DFT-B3LYP/6-311++G(d,p). Amber parameters (ff14SB force-field) were used to describe the MM environment. The sampling dynamics was performed for a total time of 10 ps using an integration time-step of 1 fs. For calculating the excitation energies, snapshots were taken at 200 fs intervals. Sampling dynamics was executed using Terachem *v1.94V*[49] interfaced with the sander module of Amber program. Excitation energies for ten low-lying states were calculated using ADC(2) with the def2-TZVP basis set using Turbomole.[44] The effect of the MM environment was included as point-charges in these calculations. The final absorption spectrum was based on the distribution of the excitation energies from 50 snapshots. Absorbance spectra was convoluted based on vertical excitation, using same approach as discussed above.

2.3 Methodological Considerations

TD-DFT methods are ubiquitous in studies of electronic structure, however they come with theoretical errors associated with energies and equilibrium geometries, which are particularly suspect in cases involving charge transfer.[37] The B3LYP functional has been routinely employed for the ground state (GS) geometry optimization in flavin systems owing to its accuracy.[33] Several studies have quantified the theoretical errors in GS bond lengths.[50–55] Furche and Ahlrichs[50] showed that DFT methods in conjunction with B3LYP are able to reproduce experimental bond-lengths with a maximum deviation of 0.02 Å, whereas Liu et al.[51] reported DFT (B3LYP) to have mean absolute errors of 0.014 Å. In another study, Tuna et al.[56] have compared TD-DFT (B3LYP) with CC2 and found that mean absolute discrepancies for C-C, C-N, and C-O bond lengths are 0.01, 0.02, and 0.038 Å, respectively.

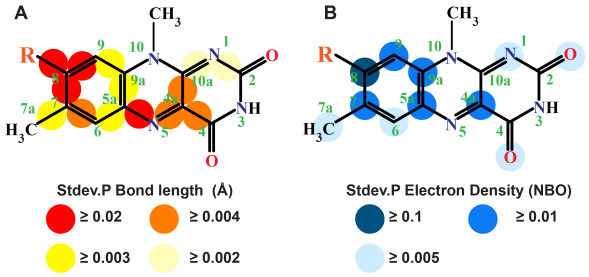

Figure 1: Bond lengths (A) and NBO atomic charges (B) most affected by substitutions at the C8 position. For each bond we calculated the standard deviation associated with the bond's length over the set of all flavin variants. Bonds that vary widely depending on R have larger standard deviations. The same procedure was applied to NBO charges to identify the atoms most responsive to the identity of R.

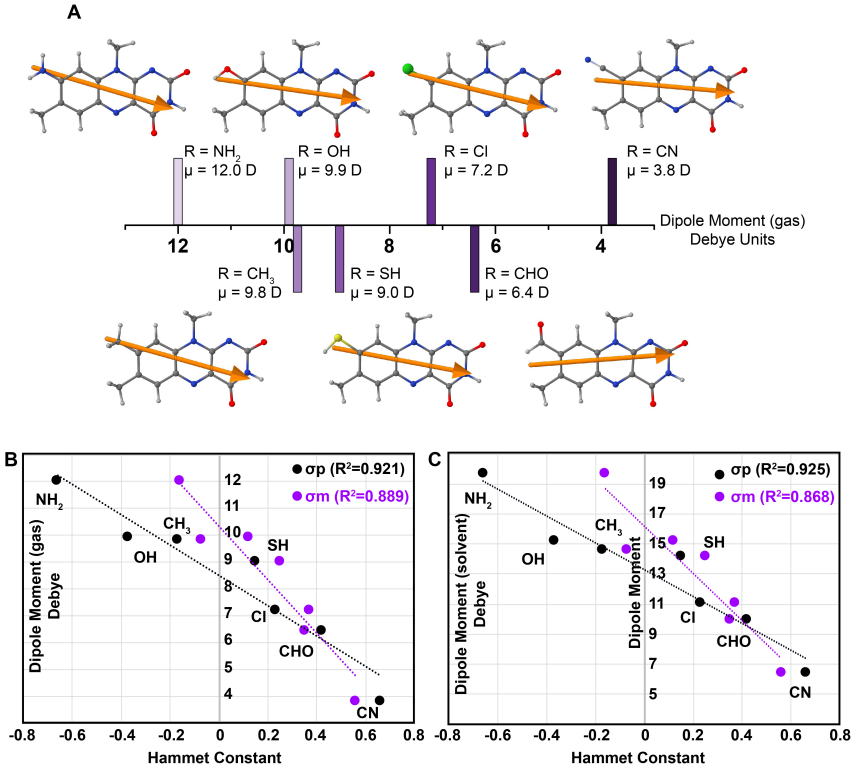

Figure 2: (A) Calculated dipole moments, μ, represented in their molecular contexts, and organized from large to small magnitudes of μ on the central scale. (B) Correlations of the dipole moments calculated in gas phase and (C) implicit solvent, with experimental Hammett constants[69] of the C8-substitutents. Plots vs. Hammett *para* or *meta* constants (σ_p and σ_m) are compared (black and magenta, respectively), to assess the significance of resonance effects that manifest in the *para* constant but much less in the *meta* constant.[69,70]

In a recent study, Wang and Durbeej[55] compared TD-DFT methods with the higher-level wavefunction method CC2

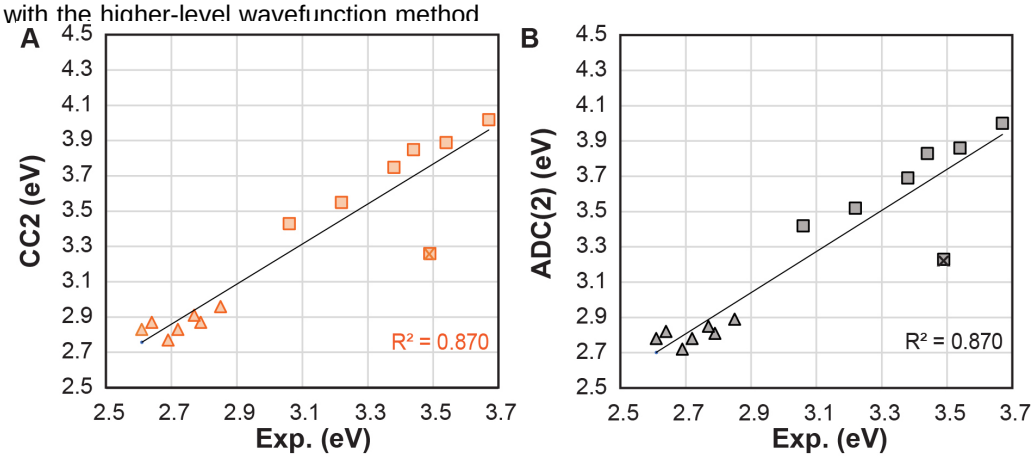

Figure 3: Correlation between experimental excitation maxima (Exp = 1240eV•nm^{-1}/λ_{max}) and calculated vertical excitation energies from wavefunction based methods (A) CC2 and (B) ADC(2)) in continuum aq. solvent model (COSMO). The transition energies corresponding to the lowest-energy bright band (band I) appear between 2.5 and 3.2 eV (triangles) whereas the energies corresponding to the second lowest-energy bright band (band II) appear between 3.0 and 4.3 eV (squares). The best fitting linear correlations are y=1.13x-0.20 and y=1.16x-33 for CC2 vs. Exp and ADC(2) vs. Exp, respectively. The standard error of regression (S) is 0.390 for A and 0.399 for B. Experimental spectra reported by Yorita *et al*., were used as the sources of many of the absorbance spectra[95] but those of 8-SH and 8-OH flavin were obtained from Ortiz-maldonado *et al.* who reported the low-pH spectra in which

compare GS and ES (excited state) bond lengths for a benchmark set containing 20 heterocyclic and substituted aromatic compounds. B3LYP has been benchmarked to calculate ES as well as GS geometries, yielding root mean squared deviations of 0.008 and 0.004 Å, respectively, relative to a higher-level method, namely CC2. Indeed, this study concluded that B3LYP is suitable for calculation of ES geometries among other DFT functionals.[55] However the fact that flavins are highly polarized raises concerns with the use of TD-DFT to describe ES energies, due to TD-DFT's documented overestimation of energies in the presence of significant net charge density.[37] To compensate, basis sets that improve the description of electron delocalization, and range-separated functionals such as CAM-B3LYP, are useful.[37,57] Alternatively, recent improvements in hardware diminish the time costs of switching to wavefunction methods. These developments are particularly important for the ESs, which are more difficult to optimize due to the gentler curvature of the potential energy surface, especially in the context of the higher energy in the excited system.

Singlet excitation energy calculations were used to benchmark *ab initio* methods including the CC2 and ADC(2), comparing their efficiency. The reported accuracies of CC2 and ADC(2) were 0.29 and 0.22 eV, respectively, for a set of organic molecules.[58,59] Furthermore, a benchmarking study on flavin in the gas-phase[60] showed that both CC2 and ADC(2) yield same order of singlet excited states, which was comparable to that obtained in earlier DFT/MRCI[61], SAC-CI[62] as well as TD-DFT studies.[63–65] Among the TD-DFT methods, the CAM-B3LYP functional reproduced the same state ordering as CC2 and ADC(2), whereas this remains an open question for the popular hybrid functional B3LYP, raising doubts as to its suitability for photochemical studies involving more than one bright state. Finally, gas-phase calculations of lumiflavin were reported to be blue

shifted relative to the experimental values and values calculated using implicit solvent.[61–64] This conclusion further motivates us to include the dielectric continuum model to improve the calculated absorption spectrum via solvent shifts.

3. Results

3.1. Long-range effects of perturbation at C8

The GS geometries of all the variants yielded bond lengths closely reproducing experimental values for LF (RMSE from experiment bond lengths was found to be 0.012 Å).[66] However, to understand how the flavin ring system can vary, differences between the different flavin variants are of interest. Comparing the standard deviation over variants for each the bonds in the flavin ring system indicates that bonds in the xylene ring are most affected (Figure 1A). This is consistent with the fact that this is the ring to which the R group is attached. Interestingly, the bond between N5 and C5a is also highly responsive. This is significant to reactivity because it is connected to the redox-active N5, and insightful regarding the electronic structure of the flavin because it is *para* to the R group. Moreover, two bonds involved in the redox-reactive diazabutadiene motif (N5-C4a-C10a-N1) are almost as responsive. These strongly affected bonds are separated by several others from the site of substitution, indicating hybridization of orbitals over considerable distances in the flavin ring system.

The changes in bond lengths in response to substitution indicate considerable redistribution of electron density. To address this directly, we compared the NBO atomic charges of heavy atoms, and these too were affected by the identity of R. Figure 1B corroborates 1A in that the atoms with the most variable NBO charges are concentrated in the xylene ring bearing R. However as with bond lengths, the remote position most affected by R but outside the xylene is an atom in the diazabutadiene motif, which is C4a. Not only does C4a participate in the flavin's redox activity, but it is the site at which O_2 attacks flavin hydroquinone and also a site of adduct formation, for example in LOV domains (light oxygen voltage domains).[67] Thus, our calculations identify the reactive regions of the flavin as those that are also particularly responsive to substitutions at position C8, despite being remote.

3.2. Molecular Dipole as an indicator of electron delocalization in the ground state

To study redistribution of electron density overall, and make additional comparisons against experimental trends, we calculated the molecular dipoles for the flavin variants. The molecular dipole moment can be thought of as charge redistribution among atoms in the GS.[68] It also demonstrates the extent to which a local entity (the R-group) alters remote functionalities of the molecule via inductive effects and orbital hybridization including mesomeric effects (resonance) in the conjugated π-system. Although some of the flavin variants are able to adopt a different tautomeric state, we studied only the tautomer with a single bond to C8, as shown in Figure 2A. The dipole moments calculated in the gas phase (Figure 2B) demonstrated the same trends as those obtained with use of implicit solvent (Figure 2C). However, the latter provide a better basis for comparison with Hammett constants because the Hammett constants are derived from experiments conducted in aqueous media.[69] For LF in water (R=CH_3), the dipole moment was calculated to be 14.6 D.

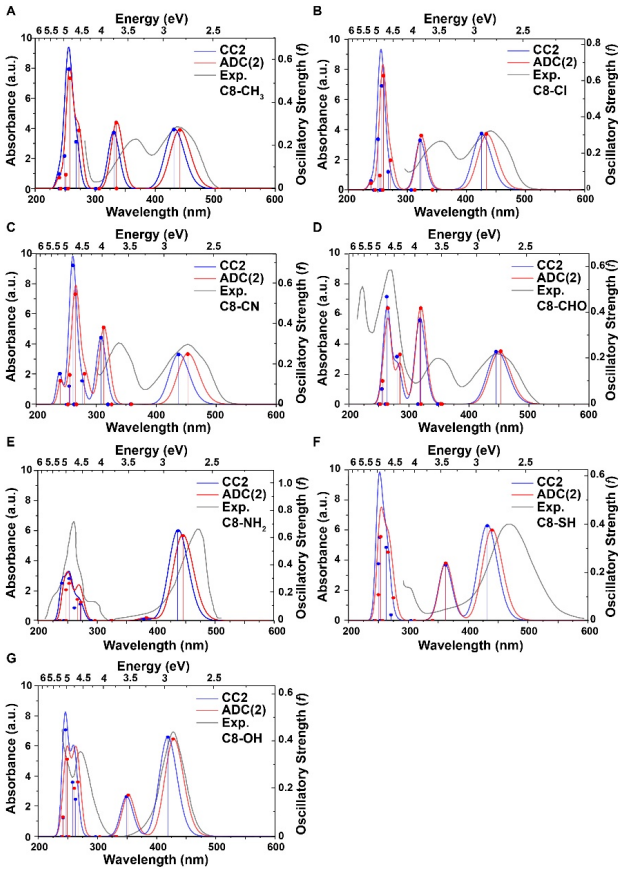

Figure 4: Calculated spectra of C8-substituted flavins with implicit solvent (COSMO) using RI-CC2 (blue) and RI-ADC(2) (red) methods. The wavelengths corresponding to vertical excitation energies are shown as sticks with heights corresponding to their oscillatory strengths. Broadening with a FWHM of 0.15 eV was used to simulate the absorbance spectra. The experimental spectra shown in grey were derived from literature reports of the flavin variants in aqueous media. Most of them were collected at neutral pH but spectra collected at low pH are shown for variants prone to deprotonation: R=SH and OH. The sources are (A) lumiflavin[97], (B) 8-Cl-flavin (Massey & colleagues [21,98,99]), (C) 8-CN-flavin (Murthy and Massey[100]), (D) 8-CHO-flavin[32,101], (E) 8-NH_2-flavin where the spectrum shown corresponds to that of 8-amino FMN.[28,102] (F) 8-SH-flavin where the experimental data were collected at pH 3.8 to ensure that the SH remained protonated[103] and also to suppress formation of the other tautomer of this variant.[104] , (G) 8-OH-flavin is also subject to tautomerization[21,96,105] thus we show experimental data collected at low pH where the effect is suppressed

The vector representations of the dipole moments indicate charge displacement from the xylene ring including the C8 position towards the uracil ring, in all cases. This is consistent with the constellation of electronegative groups in the uracil ring (left-hand side in Figure 2A). The calculations indicate relatively small variations in the dipole orientation over the series of variants. In contrast, the magnitudes of the calculated

molecular dipoles vary over a factor of three in this set of molecu
15% of th
is positio
considera
region, b
satisfying
the large
whereas
electrone
against th
and N atc

To as
experime
of the va
versus th

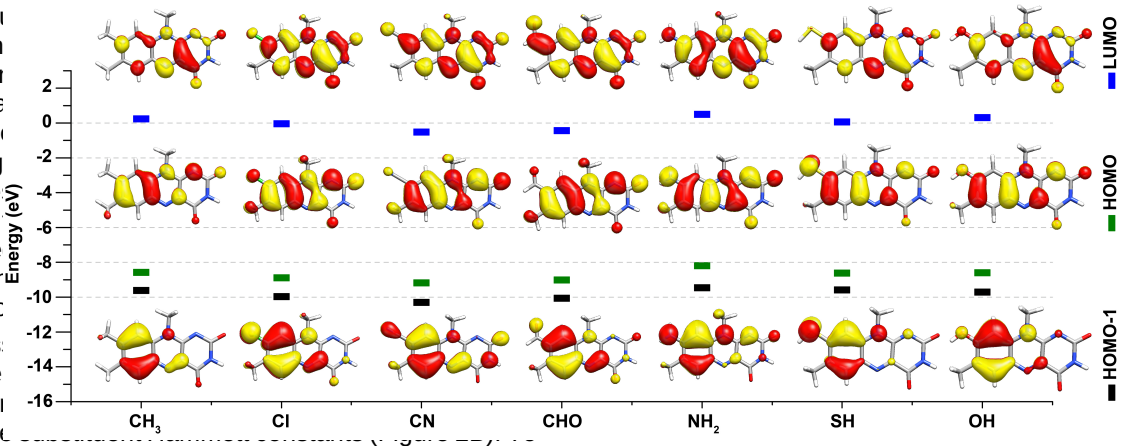

Figure 5: Comparison of MO energies (eV) for C8-substituents. The energy levels are marked by bars for the LUMO, HOMO and HOMO-1 orbitals involved in band I (HOMO → LUMO) and band II (HOMO-1 → LUMO) transitions. Please see color code at left edge.

evaluate the significance of resonance effects mediated by the π system, relative to inductive effects within the sigma framework, we compared plots vs. the *para* and *meta* Hammett constants σ_p and σ_m, respectively, because resonance effects are much more important in the former.[69,70] The adequate adherence to linearity of both the fits confirms the value of the calculations. Meanwhile, the higher quality of the linear fit to σ_p provides qualitative evidence that resonance in the π system is important in propagating electron density between C8 and the rest of the flavin. Thus, our seven C8-variants provide a challenging test of the abilities of different computational schemes to replicate delocalized flavin electronic properties.

3.3. Electronic transitions, band I ($S_0 \rightarrow S_1$), band II ($S_0 \rightarrow S_4/S_5$)

Reactivity involves not only the ground state, but low-lying excited states as well. In this section, we present CC2 and ADC(2) as the methods of choice for calculating excitation energies of flavins by comparing the latter with the experimental data. For the seven variants, the calculated excitation energies for the two lowest-energy bright transitions are compared to the measured excitation energies based on absorbance maxima, in Figure 3. Ideal agreement between calculation and experiment would yield a slope of 1.0 and R^2 approaching 1. While R^2 provides a relative measure of dependent variable variance, the standard error of regression (S) explains how far the data points are from the regression line. The units of S are those of the dependent variable, which in this case is eV. All methods produced an intercept lower than zero, indicating a constant theoretical offset that enters into calculations of individual values, but does not affect trends among the variants. Based on its slope of 1.13 and R^2 of 0.870 and S of 0.39 eV, CC2 with COSMO provides a better correlation with experimental trends than either of the gas phase approaches, where the slopes were ≥ 1.3. With implicit solvent modeled, the CC2 method yielded a slope slightly larger than the slope of 1.16 produced by the ADC(2) method, and the R^2 values were comparable.

The uniformly low R^2 values were substantially attributable to the data points representing the 8-NH_2 variant, as analysis of data sets from whence those points were removed yielded R^2 values above 0.97 for the calculations using COSMO, with the calculation vs. experiment slope being closest to 1.0 for CC2, which was accompanied by a value of S of only 0.18 eV. (Supporting Information, Figure S1). Similarly, the 8-amino variant of ethyl flavinium cation was found to display electronic properties distinct from those of variants with other substitutions at position 8, or substitutions including the amine at position 7.[71] Thus both methods are good, in combination with COSMO, and CC2 may be slightly better.

3.4. Assessment of calculated electronic spectra

The calculated absorption spectra and their experimental counterparts are shown in Figure 4 for all flavin variants. The simulated absorbance spectra are based on ten low-lying excited states which are convoluted using Gaussian functions (FWHM 0.15 eV). The lowest-energy 'band I' excitation is a bright state involving the transition between the HOMO and LUMO, whereas the electronic states involved in band II are HOMO-1 and LUMO. Overall, the calculated vertical excitation energies were in good agreement with observed absorption maxima, for band I. However, the agreement was relatively poor for band II, in all cases.

Nevertheless, as indicated in Figure 3, the calculations did a good job of reproducing trends between variants with respect to energies. Some of the earlier spectral calculations have been restricted to the gas phase [60,63,72–74] for technical reasons. However, our findings that implicit solvent significantly improves agreement with experiment, which is in agreement with previous studies that include solvent effect either with PCM[62,64] or COSMO [61,65] models. The energetic comparison in Figure 3 is underscored by the simulated spectra in Figure 4.

For the variants with R=CH_3, Cl, CN and CHO, the intensity of band II was as high or higher than that of band I, both in experimental and calculated spectra, whereas for R=NH_2, OH and SH, band I was considerably more intense than band II in both the calculated and experimental spectra, causing them the appear quite different from those of the first set. While the calculations replicated this distinction qualitatively, they did not reproduce the full magnitude of the effect as band II was calculated to be at least one-third as strong as band I for both R=SH and R=OH whereas in the experiments it appeared to be relatively weaker and indeed was relegated to a shoulder on band I in the extreme cases of R=OH and NH_2 due also to a diminished energy separation between bands I and II. R=SH, OH and NH_2 were identified has having very different Hammett σ_p constants in water than their constants in benzene, especially NH_2.[69] Thus, our calculations reproduce a known behavior anomaly which complicates direct comparison of these substituents with others. We wondered whether the crucial distinction between R= SH, OH (

hydr

mor

2, w

und

H

stre

both

resu

elec

varia

are

com

parti

corr

MOs

can

Th

the

How

rema

ofte

Mor

thei

reactivity. The CC2 results are used as a reference and the significant electronic transitions are ordered accordingly.

The calculated gas phase energies of the lowest 10 singlet excitations for all the C8-substited flavins are in the Supporting Information (Table S2-S7), and analogous values obtained using the continuum dielectric medium (COSMO) are in supporting Tables 9-14. Among the first ten excited states, CC2 gives six A' ($\pi \rightarrow \pi^*$) and four A" ($n \rightarrow \pi^*$) transitions for LF, in the order listed in Figure 6A (top entry corresponds to lowest energy allowed transition, within each type). The corresponding MOs involved in the transitions are provided in Supporting Figures S2-S8. An exception to the ordering of transition types is seen for the C8-CHO analogue, which possesses an additional 'n' type orbital, called n(C8) (SI Figure S5), due to the lone pairs of electrons on the aldehyde O of the R-group. This results in an equal number of A' ($\pi \rightarrow \pi^*$) and A" ($n \rightarrow \pi^*$) transitions among the low-lying excited states for the R=CHO variant. Notably, LF has two dark A" transitions between (bright) bands I and II. However, in the R=-CHO variant, this energy gap accommodates the additional n-π^* type transition, resulting in three A" transitions between the two prominent A' bands. Calculations employing ADC(2) produced the same rankings as those using CC2, confirming that the results are not dependent on the method. However the numerical energies varied slightly by method, as expected.

A

CH_3	CC2	ADC(2)
$^*S_1$ A'	-0.18	-0.11
S_3 A'	-0.36	-0.34
S_5 A'	0.09	0.16
S_6 A'	-0.08	0.03
S_8 A'	0.03	0.05
$^*S_{10}$ A'	0.01	0.02
$^*S_2$ A"	0.20	0.33
S_4 A"	0.50	0.52
S_7 A"	0.51	0.68
S_9 A"	0.19	0.21

B

Cl	CC2	ADC(2)
$^*S_1$ A'	-0.03	-0.09
S_3 A'	-0.24	-0.26
S_5 A'	0.30	0.23
S_6 A'	0.03	-0.01
$^*S_8$ A'	0.09	0.04
$^*S_{10}$ A'	0.02	0.03
$^*S_2$ A"	0.31	0.31
S_4 A"	0.60	0.53
S_7 A"	0.75	0.68
S_9 A"	0.22	0.19

C

CN	CC2	ADC(2)
$^*S_1$ A'	-0.14	-0.08
S4 A'	-0.22	-0.18
S_5 A'	0.13	0.21
$^*S_7$ A'	-0.03	0.04
S_8 A'	-0.07	-0.03
$^*S_{10}$ A'	0.01	0.04
$^*S_2$ A"	0.16	0.28
$^*S_3$ A"	0.48	0.51
S_6 A"	0.49	0.67
S_9 A"	0.16	0.17

D

CHO	CC2	ADC(2)
$^*S_1$ A'	-0.13	-0.07
S_4 A'	-0.23	-0.21
S_6 A'	0.05	0.11
S_7 A'	0.11	0.18
$^*S_9$ A'	-0.06	-0.04
$^*S_2$ A"	0.20	0.24
$^*S_3$ A"	0.11	0.19
S_5 A"	0.42	0.53
S_8 A"	0.51	0.67
S_{10} A"	0.18	0.20

E

NH_2	CC2	ADC(2)
$^*S_1$ A'	-0.24	-0.15
S_2 A'	-0.46	-0.40
S_5 A'	-0.03	0.08
S_6 A'	0.08	0.06
S_7 A'	-0.13	0.02
S_9 A'	0.01	-0.01
S_3 A"	0.26	0.36
S_4 A"	0.60	0.61
S_8 A"	0.60	0.75
S_{10} A"	0.24	0.24

F

SH	CC2	ADC(2)
$^*S_1$ A'	-0.16	-0.09
S_2 A'	-0.39	-0.32
S_5 A'	0.06	0.16
S_6 A'	0.02	0.03
S_8 A'	-0.01	0.08
S_9 A'	-0.12	-0.09
S_3 A"	0.20	0.32
S_4 A"	0.52	0.54
S_7 A"	0.53	0.69
S_{10} A"	0.18	0.20

G

OH	CC2	ADC(2)
$^*S_1$ A'	-0.16	-0.10
S_2 A'	-0.41	-0.35
S_5 A'	0.14	0.22
S_6 A'	-0.01	0.01
S_8 A'	0.00	0.09
S_9 A'	-0.12	-0.08
S_3 A"	0.22	0.33
S_4 A"	0.54	0.55
S_7 A"	0.55	0.72
S_{10} A"	0.20	0.21

Figure 6: Calculated solvatochromic shifts for A' and A" transitions. The color code (blue and red) denotes the size and direction of shifts for (A) lumiflavin, (B) 8-Cl-flavin, (C) 8-CN-flavin, (D) 8-CHO-flavin, (E) 8-NH_2-flavin, (F) 8-SH-flavin, and (G) 8-OH-flavin. All values are in eV units. The excited states ordering that remain consistent in gas phase and solvent are indicated with *. The boxes in red and blue highlight the transitions which show strong solvatochromic shifts

Interestingly, the solvent environment re-orders some of the transitions with respect to energy. The S_1 state resulting from the first electronic excitation remains an A' ($\pi \rightarrow \pi^*$) type transition. However, some others exchange places in the energy ranking (see Supplemental Tables S9-S14). The magnitudes of energy changes upon inclusion of implicit solvent, i.e. the solvatochromic shifts, are color-coded in Figure 6, which also provides the numerical magnitudes (aq. solvent energy minus gas-phase energy), for the first ten transitions (A' and A"). The heat map uses blue to indicate transition energies that grow (positive change) and red for transition energies that shrink (negative change) upon inclusion of a dielectric. Both directions of change were observed, with magnitudes ranging from -0.75 eV to 0.46 eV. Interestingly, the first two bright transitions in all C8-substituents show red-shifts, with the second bright state being more sensitive than the first. For the first bright state (S_1), the maximum shift was found for the C8-NH_2 flavin, of 0.24 eV, followed by the C8-CH_3 variant with a shift of 0.18 eV. The large change applicable to C8-NH_2 flavin is consistent with the exceptional sensitivity of this substituent's Hammett constants to solvent identity.[69] Among the other $\pi \rightarrow \pi^*$ transitions, the S5 state (S7 state in C8-CHO) shows a significant blue shift. Interestingly, all the A" ($n \rightarrow \pi^*$) type transitions show consistent blue-shifts. We speculate that the n state is stabilized by higher dielectric that would make the N atoms more tolerant of the electron density from the lone pairs. Strong solvatochromic shifts are present for the second and third dark states (≥0.5 eV).

3.5. Insights from electron density differences

In an effort to understand the directions of the solvatochromic shifts, we characterized the redistribution of electron density associated with the two lowest-energy bright transitions. The electron density difference (EDD) maps in Figure 7 depict the redistribution of electron density associated with individual electronic transitions (S_n-S_0).[75] Our results are in agreement with a previous analysis on lumiflavin.[60,61] The variants display qualitatively similar EDD for band I, with transfer of ED from N1, N10, and C5a to N5 and C4a, although variants in the lower row show slightly less loss of ED at N10, especially for the R=NH_2 variant. Additionally, a small portion of electron density from C7 transfers to the C8. Meanwhile the R=CHO variant is distinguished by a small

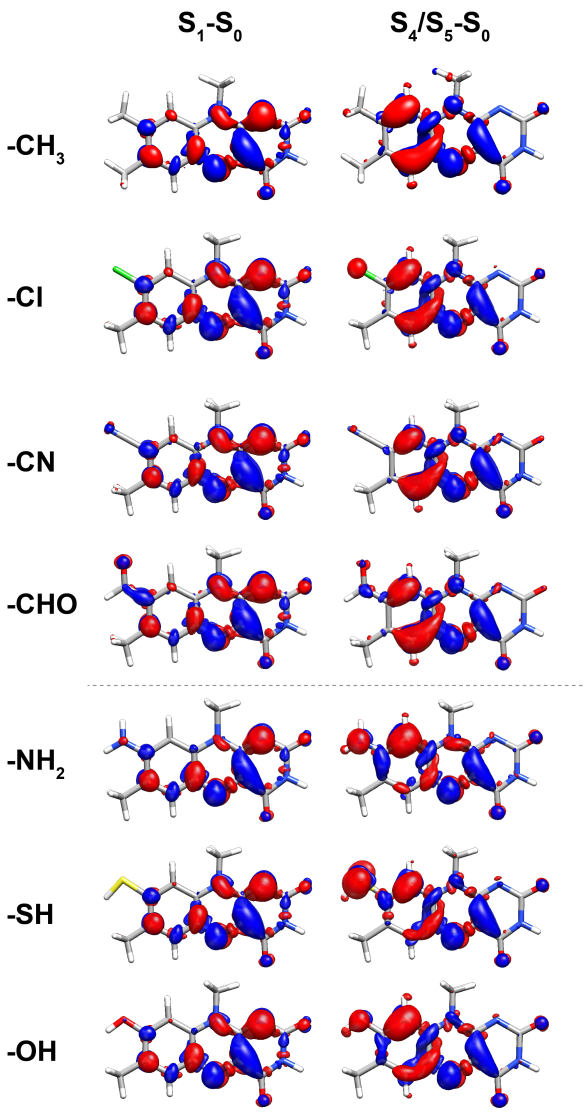

Figure 7: Plot of Electron density difference (EDD) for bands I (left) and II (right). The counter representation with blue (positive) and red (negative), denotes the excess of excited state and ground state densities, respectively. Band I's EDD is calculated as S_1-S_0, whereas band II's is calculated as S_4-S_0 except for R=CN and =CHO, where it is S_5-S_0. The dashed line separates variants with a strong band II from variants with weaker band II.

gain of ED by the functional group.

Band II EDD maps are distinct for the variants presented above the dashed line vs. those below it, in that the variants in the lower group all display transition-associated loss of ED by the R-group that is much larger than in the upper group variants, accompanied by relatively little EDD at C6 compared with the upper group. The lower group comprises the same variants that displayed the larger solvatochromic shifts for band II, in Figure 6. All variants display ED movement from the xylene ring to portions of the diazabutadiene system: N5, C4a, C9a, as well as C4, in conjunction with loss of double bond character between N5 and C4a (as when the flavin becomes reduced). However, the lower group of variants supply less of the mobile ED from the xylene ring, consistent with more ED donation from the R-group. Alone among our variants, the $R=NH_2$ variant displayed ED depletion from N10 in conjunction with band II, in a reversal of N10's moderate depletion in conjunction with band I, for this variant.

3.6. Fragment based excited-state analysis

The EDDs suggest that band II should have considerable R-to-π charge-transfer (CT) character for the lower group of variants, stronger than that in the upper group and stronger than that of band I. Since the nature and amplitude of CT informs on the ease with which ED moves in/out of the flavin ring system, it informs on the reactivity of the isoalloxazine ring, and how it may be altered by modification at the C8 position. To obtain insights for spatial extent associated with CT, we have evaluated the unrelaxed electronic density difference (D_{CT}) based on TD-DFT approaches. Interestingly, we found that the D_{CT} values are higher for band II among all the C8-flavin variants (Supporting Information Table S15). Additionally, to assess the magnitude of CT based on the wavefunction-based methods, we adopted a fragment-type approach, wherein the spatial character we tested was CT to/from R, to/from the xylene ring that subtends it (local CT) and to/from the rest of the flavin system (long-range CT). For lumiflavin, a similar analysis found that bands I and II both show significant CT character, as defined as transfer to/from the methyl on C8.

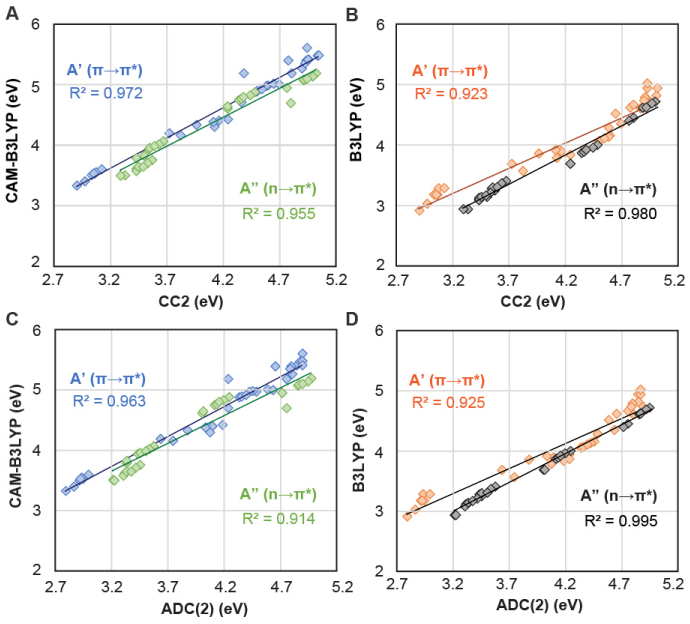

Figure 9: Comparison of ten lowest excitation energies obtained for all seven variants, distinguishing A' (π→π*) and A" (n→π*) transitions for (A) CAM-B3LYP vs. CC2, (B) B3LYP vs. CC2, (C) CAM-B3LYP vs. ADC(2), (D) B3LYP ADC(2). The R^2 and the best straight line regression are included. The equations of correlation for CC2 vs CAM-B3LYP are y=0.999x+0.419 (A') and y=0.954x+0.459 (A"); for CC2 vs B3LYP are y=0.832x+0.538 (A') and y=0.965x+0.213 (A"); for ADC(2) vs CAM-B3LYP are y=0.991x+0.564 (A') and y=0.919x+0.716 (A"); and for ADC(2) vs B3LYP are y=0.829x+0.641 (A') and y=0.958x-0.062 (A"). The comparison of A' (π→π*) transition energies is based on 34 values (5 transitions from each flavin variants except C8-CHO flavin with 4 transitions), while for A" (n→π*), 29 transitions were used (4 transitions from each flavin variant except C8-CHO flavin with 5 transitions; overall one transition was omitted compared to A' because B3LYP fails to comply the energetic ordering w.r.t. wavefunction based methods).

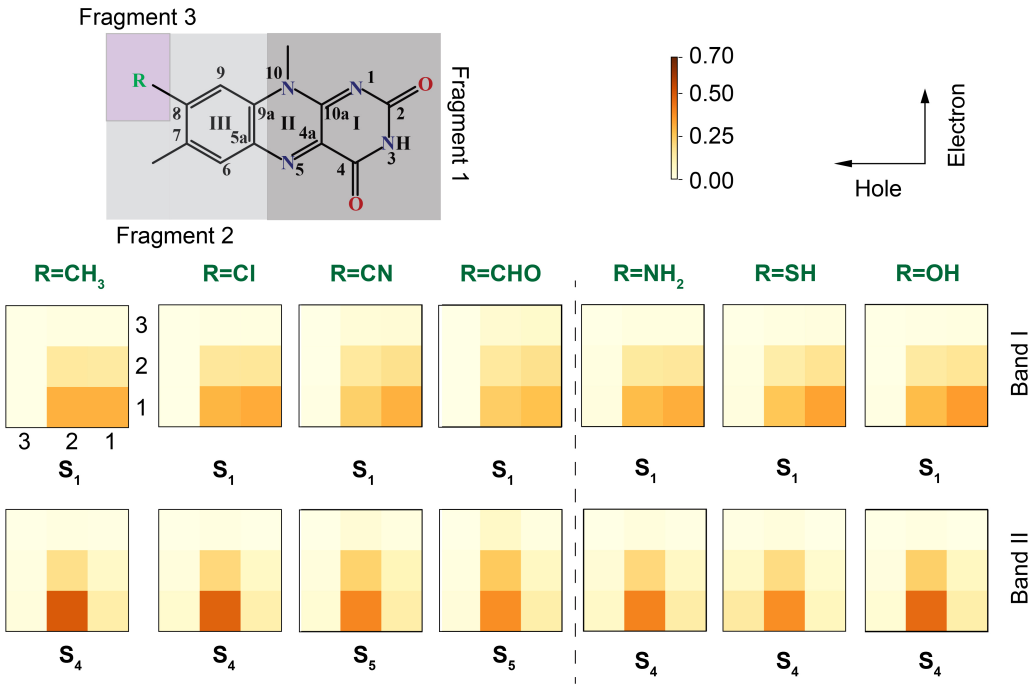

Figure 8: Hole-Electron correlation analysis of excited states distributed over three coupled fragments. Three values along each of the specify the location of the hole (x-axis) and electron (y-axis), as shown for R=CH_3 (leftmost in top row). The extent of electron-hole correlation is depicted with a color scale. Value 0.0 denotes no correlation, whereas 0.7 represents maximum electron-hole correlation.

Figure 8 provides a graphic comparison of fragment-based excited state CT analysis[43] for the different flavin variants. This method gives a picture of the distribution of electron and hole density among molecular fragments as a result of an electronic transition, revealing the dynamic correlation between individual fragments.[76] Cases when the hole and electron are in the same fragment (local excitation) manifest as intense color in a diagonal cell. CT manifests as intense coloration in off-diagonal cells positioned with one coordinate representing the location of the hole (horizontal offset) and one representing the electron (vertical offset). We defined fragments as shown in Figure 8 as the basis of our electron and hole analysis. For each flavin variant, we analyzed the excited states corresponding to band I and II.

In lumiflavin for band I, the dominant electron transfer is from fragment 2→1, with less 1→2 transfer. All seven variants display the same CT pattern, but only in LF is band I CT as strong as 1→1 local excitation under our fragmentation scheme. For band II, intense CT from fragment 2→1 is stronger than local excitation in all cases, consistent with the xylene to diazabutadiene transfer noted in connection with Figure 7. A hole contribution from the R group (fragment 3) is visible in the case of band II for C8=SH, and very weakly for C8-NH_2 and C8-OH. Overall, these results highlight CT from fragment 2 to fragment 1 specifically in connection with band II Figure 7.

The fragment analysis facilitates quantification of CT character, so a scheme identifying the R-group alone as one fragment and the rest of the flavin as the other, was also used to calculate R-to-flavin CT (Table 1). Consistent with the qualitative analyses above, band II shows greater CT character than band I for all variants. Particularly for the cases of R=Cl and R=SH, the CT value of band II is > 3 times that of band I. We note that atoms S and Cl are both electron-rich third-row elements whereas all the other substituents place second-row elements in contact with the flavin π system. Thus, it seems possible that more extended 3s and p orbitals may mediate CT via the sigma framework in conjunction with band II. The strong band II CT character for all variants (relative to band I) argues in favor of mediation via features shared by all. On the other hand, the R=CHO variant alone shows strong CT character for band I, consistent with the EDD map in Figure 7 and the fact that this substituent extends the π system (CN does too, and has the second highest band I CT). For both bands, CT character varies over a factor of 4 within our set of only seven flavin variants, identifying CT character as extremely responsive to the substituents at position C8.

Table 1: R-to-flavin Charge Transfer (CT) for band I and band II.[a]

R group	CT Band I ($S_0 \rightarrow S_1$)	CT Band II ($S_0 \rightarrow S_4/S_5$)
CH_3	0.031	0.057
Cl	0.029	0.089
CN	0.086	0.123
CHO	0.113	0.132

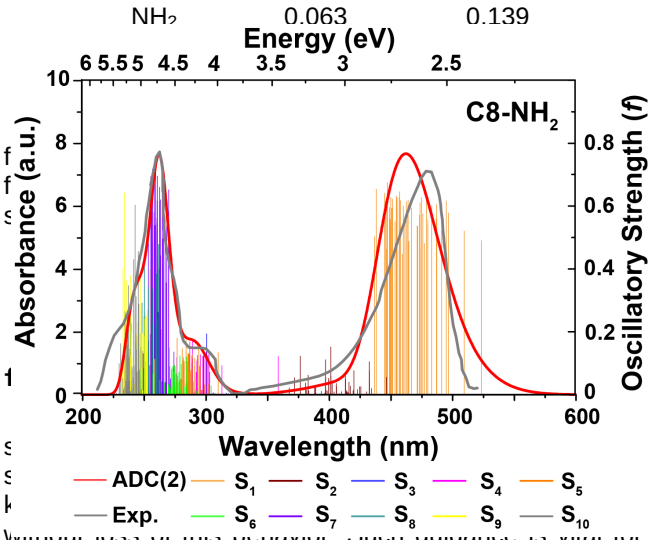

Figure 10: Calculated absorbance spectra of C8-amino flavin from QM/MM trajectory in explicit solvent box (TIP3P water models). The resulting calculated spectrum is in red, and compared with experimental spectrum in grey.[28,77] The plot shown is average of 50 snapshots, where the individual vertical excitation energies for ten low-lying excited states are shown as sticks. Excitation energies were calculated with ADC(2)/def2-TZVP//AMBER level of theory.

Interestingly, the above indicates no different outcomes for R=NH_2 than for the other variants, so it does not shed light on the anomalous behavior of the R=NH_2 variant in our regression of calculated excitation energies vs. experiment. In Figure 3, the correlation was not improved by the use of implicit solvent, whereas the Hammett constants of the amine group are known to vary more with solvent identity than those of other substituents.[69] However the three variants with the largest solvatochromism for band II are also those with the most CT associated with band II, and band II is less well replicated by the conventional approaches in Figure 4, suggesting possible significance of molecular interactions between the R-group and the solvent. Therefore, we explored the effect of explicit treatment of solvent. Prior work used a limited number of water molecules at key positions, but the geometry of the compound and the waters' positions relative to it were not allowed to evolve.[77] Thus, the obtained spectra could be biased due to the starting structures used. In contrast, we provided full hydration of our 8-NH_2 flavin in a water box and allowed the solvent as well as the flavin to equilibrate before capturing snapshots reflecting the fluctuations among accessible Wigner conformations (See Supporting Information Figure S10). Although CC2 was shown to be the best method overall for treating the flavins (Figure 3), ACD(2) is more economical and Figure 4E shows that it does slightly better than CC2 for the particular case of R=NH_2. Therefore each of the snapshots was used as the basis for ADC(2) calculation of an electronic spectrum and the results were summed to produce a conformationally averaged spectrum for comparison with experimental data, in Figure 10.

Figure 10 demonstrates a good agreement with experiment, and a significant improvement over the implicit solvent results shown in Figure 4E. The QM/MM sampling allows us to explain the experimental absence of vibrational structure (shoulders or gaussian broadening) on band I for this variant, although structure is discernable as shoulders for the R=CH_3, Cl, CN and CHO variants. Figure 10 also shows that the energy of the S_1 transition varies over a large range in the different snapshots indicating enormous sensitivity to details of the molecular interactions with water. The energy range of the S_1 transition thus exceeds the magnitude of vibrational splitting and prevents resolution of the latter. The conformational broadening we observe requires that QM/MM sampling be undertaken, to correctly replicate the breadth of this electronic absorption. Nevertheless, the asymmetry of the S_1 peak might also reflect vibronic effects. Specific treatment of these would require additional theoretical efforts, to obtain vibrationally resolved spectra (e.g. consideration of Huang-Rhys vibronic coupling.[79] However, our QM/MM sampling method provides a simple unbiased means of sampling geometries accessed by the vibrations and accurately reproduces the structure observed at shorter wavelengths, which was not reproduced by ADC(2) or CC2 calculations, using a single lowest energy conformation

4.3. Success in reproducing chemical trends

Our study exploits an empirical predictor that has proven to correlate with a remarkable variety of

efforts underway to model flavins in complicated protein systems, where computational simplifications are often essential, yet covalent modifications are also important. Following the example of work from Thiel's group[77], we used CC2 with the COSMO model as a reference. The use of post-Hartree-Fock methods (CC2 and ADC(2)) also serves to approximate effects of electron correlation, the key to improving the accuracy of vertical excitation energy calculations.[78] In what follows, we assess the extent to which less demanding computational approaches can achieve the same results. We chose DFT due to its widespread use and compared its performance in conjunction with the popular hybrid functional B3LYP, or the range-separated version: CAM-B3LYP. To avoid additional complexity, gas-phase calculations were compared, with reference to the excitation energies for the ten lowest-lying excited states. Error analysis of excitation energies calculated in the gas phase using TD-DFT methods w.r.t. to the experimental data are shown in the Supporting Information Figure S9.

Figure 9 shows that the CAM-B3LYP excitation energies are generally higher than their CC2 counterparts. The same is true vs. a reference of ADC(2) (Figures 9A, C). When simple B3LYP was used we found the opposite: the TD-DFT energies were generally lower than those obtained by the wavefunction methods, with the significant exception that the first bright transition was slightly high in energy. More importantly, B3LYP was problematic in that its energetic ordering of the excited states, differed from that produced by the higher-order method CC2, as well as the range-separated DFT functional. Thus, the number of A' vs. A" transitions was not same among the first ten excited states calculated using B3LYP, as when CC2 was used, or even with CAM-B3LYP. Finally, CAM-B3LYP yielded a tighter correlation with wavefunction methods than does B3LYP, for A' transitions. However, the opposite is observed for A" transitions (Fig 9 A and B). Overall, either the B3LYP or CAM-B3LYP functional could be used for the lowest energy excitation, but if TD-DFT is to be used in more comprehensive studies then the CAM-B3LYP functional should be used.

4.2. Improved spectral calculation with QM/MM sampling

phenomena: the Hammett constant.[69] Within series of similar aromatic compounds, properties ranging from proton dissociation energy, to susceptibility to hydrolysis, and absorption maxima trend with the Hammett constant of a substituent that is varied while the rest of the molecule is held constant. The set flavins compared herein correspond to such a series, so our finding that calculated dipole moments trend with the Hammett constant corresponds to a replication of experimental behaviour. Hammett constants reflect three dominant contributions[70]: -1- electron density redistribution via the sigma framework due to the substituent's electronegativity (inductive effects), -2- electron density redistribution via π bonding resonance effects (mesomeric effects), and -3- Coulomb effects. When the varied substituent is *para* to the position whose reactivity is being measured, the Hammett *para* constant 'σ_p' applies and reflects all 3 contributions, but when the same substituent is *meta* to the reactive position σ_m is in effect, reflecting primarily contributions 1 and 3. Our finding that computed molecular dipoles trend better with σ_p than σ_m indicates that mesomeric effects of the π system are involved in propagating the R-group's influence through the flavin system as a whole.

The position that is *para* to C8 is C5a and indeed C5a's bond length to the next ring in the flavin changes much more than the analogous meta bond, from C9a (Figure 1A). Bond lengths reflect bond order, which in this case corresponds to extent of π character present in addition to the struc
responsi
σ_p than
the π sy
relatively
charges
though it
attached

The H
in which
are less
which d
system.
and beha
at the ot
the findir
adjacent
electron
length a
flavin, ar
to ident
correlati
ground s
characte
the flavi
diazabut
the two
the cova
can eng
N5 and the bridge via N10. Figure 11 shows that more negative σ_p (electron donating) substituents produce consistently lower BLAs (higher electron correlation) within the diazabutadiene, as well as between the xylene and uracil rings via the N5 bridge. The N10 bridge does not appear to mediate much variable coupling between the two rings (all three graphs employ the same vertical scale). We propose that electron donating substituents produce the most extensive correlation because they are best able to satisfy or compensate for the inherent electronegativity of the uracil ring, creating a push-pull system of sorts. More generally, we see how modification at a single position can tune the electronic nature of the system.

4.5 Significance of the 8-position

Given the leverage of the 8-position substituent on the redox active diazabutadiene, via the flavin π system, it is no coincidence that life has repeatedly modified the 8 position of naturally occurring flavins.[3] Moreover, two better-known flavin analogs retained through evolution are modified at the 8 position: roseoflavin bears $N(CH_3)_2$ while F420 has OH (and C5). We note that the reciprocal nature of the electronic coupling we document between the 8 position and the rest of the flavin explains why perturbation elsewhere in the flavin affects the reactivity of the C8.[1] Furthermore our calculations show that the nature of the 8-position substituent qualitatively affects the nature of the response produced in the flavin electronic structure. The substituents with non-bonding lone pairs: NH_2, OH and SH were found to resemble one another in producing band II amplitude lower than the amplitude of band I, in agreement with experimental spectra (Fig. 4). We can correlate this with shared

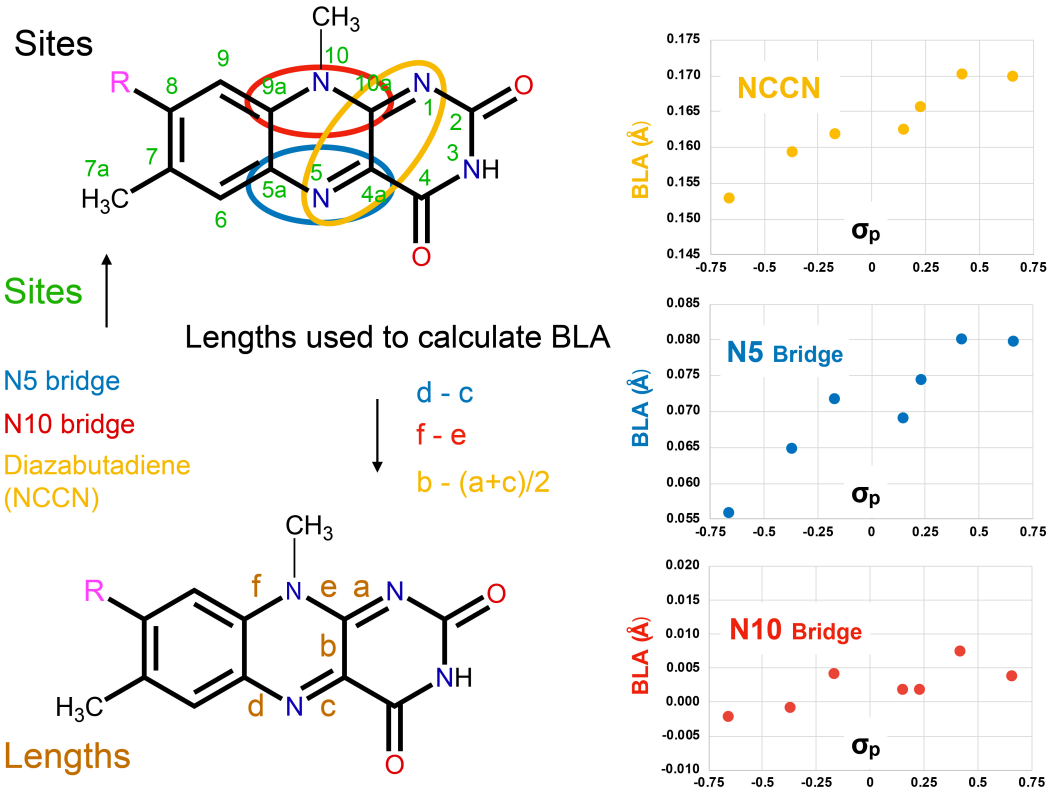

Figure 11: Trends in degree of electron correlation over the flavin ring, as revealed by BLA vs. the Hammett constant, σ_p of the substituent at C8 (R). Flavin is viewed from the *si* face.

underlying CT character. The electron density difference maps show migration of electron density from the 8 substituents with non-bonded lone pair to the rest of the molecule in conjunction with band II absorption (Fig. 8).

Additional studies are needed to determine whether other positions at which modifications are common are also strongly correlated to the body of the ring, for example the C6. Moreover, once a modification is installed, our work demonstrates that the host protein will have altered the reactivity of its flavin. The electron rich Cys, Tyr and His residues that commonly attack at position 8 can be likened to our substituents with negative σ_p values, and so we predict their flavins will be more correlated. Covalent modifications at the 8 position produced shifts in the flavin reduction midpoint potential that trended with the substituent Hammett constants.[84] Moreover, the modulation of these ground state properties is complemented by the important trends revealed in the energies and CT natures of excitations, in Figures 7 and 8, and Table 1.

5 Concluding Remarks and Implications for applications

The countless biochemical roles played by flavins are a testimony to its chemical virtuosity and versatility. Here we begin to understand this in terms of interplays between the different positions on the flavin ring and over the system. However, flavin's utility has already been appreciated based on empirical efforts, and elegant studies have employed flavins immobilized on electrodes or carbon nanotubes[85] as well as in a mobile phase of batteries.[86] Moreover, the electronic transitions we calculated are also being exploited in cases where flavins are in use as sensitizers for photochemical cell,[85,87,88] or sensors.[89] While proteins tune flavin reactivity via multiple non-covalent interactions, we have demonstrated that even modification at a single position can change the way electron density is redistributed within the molecule as well as the associated energies. This covalent tunability is more portable than that produced by proteins and is also more permanent.[87,90] Thus, current computational insights into the reactivities of different flavin variants, in conjunction with established synthetic routes offers to device and materials engineers a broad and nuanced flavin palette applicable to electrochemical and photochemical applications.[91]

We have rationalized the effects of covalent modifications of flavin at the C8 position by applying a combination of quantum chemical methods. The substitution at C8 shows the potential to affect geometrical parameters and NBO charges locally on the xylene ring, and also displays a long-range effect on flavin reactivity via the diazabutadiene motif (N5-C4a-C10a-N1). Furthermore, the calculated dipole moments show a good correlation with experimental *para*-Hammett constants (σ_p). Such findings not only validate our calculations but also explain the long range effects of substitution at C8 in terms of the conjugated π system.

Our calculations also account for the C8 substituent's effects on absorbance spectra of modified flavins. We have shown that the electronic spectra calculated with higher-order methods such as RI-CC2 and RI-ADC(2) more accurately capture the spectral shifts. Although B3LYP and CAM-B3LYP perform well for the lowest-energy transition, the excited state ordering and the corresponding shift in state energetics do not reproduce the results of wave function methods, so the latter should be used to simulate complete spectra and to study photochemical reactions. Three of the variants displayed stronger band II solvatochromism and CT, raising the possibility that they are affected by discrete interactions with water molecules. Indeed conformational sampling in an explicit water box with a QM/MM approach reproduced the experimental spectrum of the most challenging variant: 8-amino flavin. The requirement for explicit solvent and the distribution of energies obtained from different snapshots can explain the sensitivity of the electronic transitions to the flavin environment, including extreme peak broadening and related low maximal peak amplitudes, in the variants with R=NH_2, OH, or SH.

The greater responsiveness of band II ($S_0 \rightarrow S_4/S_5$) than band I ($S_0 \rightarrow S_1$) can be understood in terms of the greater of loss of ED from the R group associated with the former transition ($S_0 \rightarrow S_4$). Indeed, multiple different assessments of CT character concur that band II in more active in this regard than band I, consistent with Stark spectroscopy.[92] Nevertheless, the R group has a strong influence on determining the fate electron transfer from the local xylene ring to the uracil ring and diazabutadiene motif. This information is transferable to the protein environment for understanding the differential reactivity of chemically modified flavins. Furthermore, the detailed analysis presented on the electronic structure can guide development of novel flavin-based light-utilizing materials with desired spectral properties.[89,93,94]

ASSOCIATED CONTENT

Supporting Information

The Supporting Information is available free of charge on the ACS Publications website. Details of calculated dipole moment, vertical excitation energies, and molecular orbitals involved in electronic transitions are in the Supplementary Information (PDF)

AUTHOR INFORMATION

Corresponding Author

*****E-mail: andrea.mroginski@tu-berlin.de for M.-A.M. and afmill3r2@gmail.com for A.-F.M**.**

NOTES

The authors declare no competing financial interest.

DATA AND SOFTWARE STATEMENT

Gaussian v16 package (https://gaussian.com/gaussian16/), Turbomole software (https://www.turbomole.org/), Chimera program (https://www.cgl.ucsf.edu/chimera/), Theodore package (https://theodore-qc.sourceforge.io/), Terachem package (http://www.petachem.com/products.html). All data to reproduce the theoretical calculations are included in the Supporting Information.

ACKNOWLEDGMENT

R.K.K. and A.-F. M. thank the Einstein Foundation of Berlin for support. Aspects of the work described were supported by the National Science Foundation, Chemistry of Life Processes CHE-1808433. M.A.M. thanks the Deutsche Forschungsgemeinschaft (DFG, German Research Foundation) under Germany's Excellence Strategy—EXC 2008-390540038-UniSysCat for funding**.** The authors thank to Vikram Gazula of University of Kentucky and Sebastian Kraus of Technische Universität Berlin for providing technical support of computing facilities**.** RKK dedicates this paper to Annapurna Kar in recognition of wisdom and guidance over the years.

REFERENCES

ADDIN Mendeley Bibliography CSL_BIBLIOGRAPHY (1) Heuts, D. P. H. M.; Scrutton, N. S.; Mcintire, W. S.; Fraaije, M. W. What's in a Covalent Bond ? On the Role and Formation of Covalently Bound Flavin Cofactors. *FEBS J.* **2009**, *276*, 3405–3427. https://doi.org/10.1111/j.1742-4658.2009.07053.x.

(2) Mewies, M.; Mcintire, W. S.; Scrutton, N. S. Covalent Attachment of Flavin Adenine Dinucleotide (FAD) and Flavin Mononucleotide (FMN) to Enzymes: The Current State of Affairs. *Protein Sci.* **1998**, No. 7, 7–20.

(3) Birrell, J. A.; Hirst, J. Investigation of NADH Binding, Hydride Transfer , and NAD+ Dissociation during NADH Oxidation by Mitochondrial Complex I Using Modified Nicotinamide Nucleotides. *Biochemistry* **2013**, *52*, 4048–4055.

(4) Ghisla, S.; Thorpe, C. Acyl-CoA Dehydrogenases A Mechanistic Overview. *Eur. J. Biochem.* **2004**, *271*, 494–508. https://doi.org/10.1046/j.1432-1033.2003.03946.x.

(5) Oubayashi, D. D.; Otake, T. O.; Aeda, Y. M.; Ki, M. O.; Okunaga, Y. T.; Akurai, A. S.; Agaosa, Y. N.; Ikami, B. M.; Chida, H. U. Formate Oxidase , an Enzyme of the Glucose-Methanol-Choline Oxidoreductase Family , Has a His-Arg Pair and 8-Formyl-FAD at the Catalytic Site. *Biosci. Biotechnol. Biochem.* **2011**, *75* (9), 1662–1667. https://doi.org/10.1271/bbb.110153.

(6) Massey, V.; Gantherf, H. On the Interpretation of the Absorption Spectra of Flavoproteins with Special Reference to D-Amino Acid Oxidase. *Biochemistry* **1965**, *4* (6), 1161–1173.

(7) Huijbers, M. M. E.; Montersino, S.; Westphal, A. H.; Tischler, D.; Berkel, W. J. H. Van. Flavin Dependent Monooxygenases. *Arch. Biochem. Biophys.* **2014**, *544*, 2–17. https://doi.org/10.1016/j.abb.2013.12.005.

(8) Augustin, P.; Toplak, M.; Fuchs, K.; Gerstmann, E. C.; Prassl, R.; Winkler, A.; Macheroux, P. Oxidation of the FAD Cofactor to the 8-Formyl-Derivative in Human Electron-Transferring Flavoprotein. *J. Biol. Chem.* **2018**, *293* (i), 2829–2840. https://doi.org/10.1074/jbc.RA117.000846.

(9) Drennan, C. L.; Pattridge, K. A.; Weber, C. H.; Metzger, A. L.; Hoover, D. M.; Ludwig, M. L.; Arbor, A. Refined Structures of Oxidized Flavodoxin from Anacystis Nidulans. *J. Mol. Biol.* **1999**, *294*, 711–724.

(10) Setser, J. W.; Heemstra, J. R.; Walsh, C. T.; Drennan, C. L. Crystallographic Evidence of Drastic Conformational Changes in the Active Site of a Flavin-Dependent N-Hydroxylase. *Biochemistry* **2014**, *536063–607*.

(11) Joosten, V.; van Berkel, W. J. Flavoenzymes. *Curr. Opin. Chem. Biol.* **2007**, *11* (2), 195–202. https://doi.org/10.1016/j.cbpa.2007.01.010.

(12) Tweedy, S. E.; Rodr, A.; Narayan, A. R. H.; Zimmerman, P. M.; Brooks III, C. L.; Wymore, T. Hydroxyl Radical-Coupled Electron-Transfer Mechanism of Flavin-Dependent Hydroxylases. *J. Phys. Chem. B* **2019**, *123*, 8065–8073. https://doi.org/10.1021/acs.jpcb.9b08178.

(13) Hense, A.; Herman, E.; Oldemeyer, S.; Kottke, T. Proton Transfer to Flavin Stabilizes the Signaling State of the Blue Light Receptor Plant Cryptochrome. *J. Biol. Chem.* **2015**, *290* (3), 1743–1751. https://doi.org/10.1074/jbc.M114.606327.

(14) Kottke, T.; Heberle, J.; Hehn, D.; Dick, B.; Hegemann, P. Phot-LOV1 : Photocycle of a Blue-Light Receptor Domain from the Green Alga Chlamydomonas Reinhardtii. *Biophys. J.* **2003**, *84* (2), 1192–1201. https://doi.org/10.1016/S0006-3495(03)74933-9.

(15) Domratcheva, T.; Hartmann, E.; Schlichting, I.; Kottke, T. Evidence for Tautomerisation of Glutamine in BLUF Blue Light Receptors by Vibrational Spectroscopy and Computational Chemistry. *Sci. Rep.* **2016**, *6* (February), 1–14. https://doi.org/10.1038/srep22669.

(16) Kodali, G.; Siddiqui, S. U.; Stanley, R. J. Charge Redistribution in Oxidized and Semiquinone E . Coli DNA Photolyase upon Photoexcitation: Stark Spectroscopy Reveals a

Rationale for the Position of Trp382. *J. Am. Chem. Soc.* **2009**, No. 131, 4795–4807.

(17) Murgida, D. H.; Schleicher, E.; Bacher, A.; Richter, G.; Hildebrandt, P. Resonance Raman Spectroscopic Study of the Neutral Flavin Radical Complex of DNA Photolyase from Escherichia Coli. *J. Raman Spectrosc.* **2001**, *32*, 551–556.

(18) Heyes, D. J.; Lakavath, B.; Hardman, S. J. O.; Sakuma, M.; Hedison, T. M.; Scrutton, N. S. Photochemical Mechanism of Light-Driven Fatty Acid Photodecarboxylase. *ACS Catal.* **2020**, *10* (12), 6691–6696. https://doi.org/10.1021/acscatal.0c01684.

(19) Mukherjee, A.; Rokita, S. E. Single Amino Acid Switch between a Flavin-Dependent Dehalogenase and Nitroreductase. *J. Am. Chem. Soc.* **2015**, *137*, 15342–15345. https://doi.org/10.1021/jacs.5b07540.

(20) Wiltschko, R.; Ahmad, M.; Nießner, C.; Gehring, D.; Wiltschko, W. Light-Dependent Magnetoreception in Birds: The Crucial Step Occurs in the Dark. *J. R. Soc. Interface* **2016**, No. 13, 20151010.

(21) Massey, V.; Hemmerichs, P. Active-Site Probes of Flavoproteins. *Biochem. Soc. Trans.* **1980**, *8*, 246–257.

(22) Haynes, C. A.; Koder, R. L.; Miller, A.; Rodgers, D. W. Structures of Nitroreductase in Three States. *J. Biol. Chem.* **2002**, *277* (13), 11513–11520. https://doi.org/10.1074/jbc.M111334200.

(23) Lennon, B. W.; Williams, C. H.; Ludwig, M. L. Crystal Structure of Reduced Thioredoxin Reductase from Escherichia Coli: Structural Flexibility in the Isoalloxazine Ring of the Flavin Adenine Dinucleotide Cofactor. *Protein Sci.* **1999**, *8*, 2366–2379.

(24) Mohamed-Raseek, N.; Duan, H. D.; Hildebrandt, P.; Mroginski, M. A.; Miller, A. F. Spectroscopic, Thermodynamic and Computational Evidence of the Locations of the FADs in the Nitrogen Fixation-Associated Electron Transfer Flavoprotein. *Chem. Sci.* **2019**, *10* (33), 7762–7772. https://doi.org/10.1039/c9sc00942f.

(25) Wongnate, T.; Surawatanawong, P.; Visitsatthawong, S.; Sucharitakul, J.; Scrutton, N. S.; Chaiyen, P. Proton-Coupled Electron Transfer and Adduct Con Fi Guration Are Important for C4a-Hydroperoxy Fl Avin Formation and Stabilization in a Flavoenzyme. *J. Am. Chem. Soc.* **2014**, *136*, 241–253.

(26) Goyal, P.; Hammes-Schiffer, S. Role of Active Site Conformational Changes in Photocycle Activation of the AppA BLUF Photoreceptor. *Proc. Natl. Acad. Sci. U. S. A.* **2017**, *114* (7), 1480–1485. https://doi.org/10.1073/pnas.1621393114.

(27) Yorita, K.; Matsuoka, T.; Misaki, H.; Massey, V. Interaction of Two Arginine Residues in Lactate Oxidase with the Enzyme Flavin: Conversion of FMN to 8-Formyl-FMN. *Proc. Natl. Acad. Sci. USA* **2000**, *97* (24), 13039–13044.

(28) Jhulki, I.; Chanani, P. K.; Abdelwahed, S. H.; Begley, T. P. A Remarkable Oxidative Cascade That Replaces the Riboflavin C8 Methyl with an Amino Group during Roseoflavin Biosynthesis. *J. Am. Chem. Soc.* **2016**, *138*, 8324–8327. https://doi.org/10.1021/jacs.6b02469.

(29) Gorelick, R. J.; Thorpe, C. Electron-Transferring Flavoprotein from Pig Kidney: Flavin Analogue. *Biochemistry* **1986**, *25*, 7092–7098.

(30) Thibodeaux, C. J.; Chang, W.; Liu, H. Unraveling Flavoenzyme Reaction Mechanisms Using Flavin Analogues and Linear Free Energy Relationships. *Methods Enzymol.* **2019**, *620*, 167–188. https://doi.org/10.1016/bs.mie.2019.03.010.

(31) Robbins, J. M.; Geng, J.; Barry, B. A.; Gadda, G.; Bommarius, A. S. Photoirradiation Generates an Ultrastable 8-Formyl FAD Semiquinone Radical with Unusual Properties in Formate Oxidase. *Biochemistry* **2018**, *57*, 5818–5826. https://doi.org/10.1021/acs.biochem.8b00571.

(32) Doubayashi, D.; Oki, M.; Mikami, B.; Uchida, H. The Microenvironment Surrounding FAD Mediates Its Conversion to 8-Formyl-FAD in Aspergillus Oryzae RIB40 Formate Oxidase. *J. Biochem.* **2019**, *166* (1), 67–75. https://doi.org/10.1093/jb/mvz009.

(33) Kar, R. K.; Miller, A.-F.; Mroginski, M. A. Understanding Flavin Electronic Structure and Spectra. *WIREs Comput. Mol. Sci.* **2021**, e1541.

(34) Klamt, A.; Moya, C.; Palomar, J. A Comprehensive Comparison of the IEFPCM and SS(V)PE Continuum Solvation Methods with the COSMO Approach. *J. Chem. Theory Comput.* **2015**, *11* (9), 4220–4225. https://doi.org/10.1021/acs.jctc.5b00601.

(35) Frisch, M. J.; Trucks, G. W.; Schlegel, H. B.; Scuseria, G. E.; Robb, M. A.; Cheeseman, J. R.; Scalmani, G.; Barone, V.; Petersson, G. A.; Nakatsuji, H. *et al.* G16 Revision C.01, Gaussian, Inc., Wallingford CT., 2016. **2016**.

(36) Hättig, C. Structure Optimizations for Excited States with Correlated Second-Order Methods: CC2 and ADC(2). *Adv. Quantum Chem.* **2005**,

50 (2), 37–60. https://doi.org/10.1016/S0065-3276(05)50003-0.

(37) Adamo, C.; Jacquemin, D. The Calculations of Excited-State Properties with Time-Dependent Density Functional Theory. *Chem. Soc. Rev.* **2013**, *42* (3), 845–856. https://doi.org/10.1039/c2cs35394f.

(38) Becke, A. D. Density-Functional Thermochemistry. III. The Role of Exact Exchange. *J. Chem. Phys.* **1993**, *98* (7), 5648–5652. https://doi.org/10.1063/1.464913.

(39) Yanai, T.; Tew, D. P.; Handy, N. C. A New Hybrid Exchange-Correlation Functional Using the Coulomb-Attenuating Method (CAM-B3LYP). *Chem. Phys. Lett.* **2004**, *393* (1–3), 51–57. https://doi.org/10.1016/j.cplett.2004.06.011.

(40) Rhee, Y. M.; Head-Gordon, M. Scaled Second-Order Perturbation Corrections to Configuration Interaction Singles: Efficient and Reliable Excitation Energy Methods. *J. Phys. Chem. A* **2007**, *111* (24), 5314–5326. https://doi.org/10.1021/jp068409j.

(41) Khani, K. S.; A.M., K.; Hattig, C. COSMO-RI-ADC(2) Excitation Energies and Excited State Gradients. *Phys. Chem. Chem. Phys.* **2018**, *20* (16354–16363). https://doi.org/10.1039/c8cp00643a.

(42) Huang, C. C.; Meng, E. C.; Morris, J. H.; Pettersen, E. F.; Ferrin, T. E. Enhancing UCSF Chimera through Web Services. *Nucleic Acids Res.* **2014**, *42* (May), 478–484. https://doi.org/10.1093/nar/gku377.

(43) Plasser, F. TheoDORE : A Toolbox for a Detailed and Automated Analysis of Electronic Excited State Computations. *J. Chem. Phys.* **2020**, *152* (February), 084108. https://doi.org/10.1063/1.5143076.

(44) Balasubramani, S. G.; Chen, G. P.; Coriani, S.; Diedenhofen, M.; Frank, M. S.; Franzke, Y. J.; Furche, F.; Grotjahn, R.; Harding, M. E.; Hättig, C. *et al.* TURBOMOLE: Modular Program Suite for Ab Initio Quantum-Chemical and Condensed-Matter Simulations. *J. Chem. Phys.* **2020**, *152* (18). https://doi.org/10.1063/5.0004635.

(45) Maschietto, F.; Campetella, M.; Frisch, M. J.; Scalmani, G.; Adamo, C.; Ciofini, I. How Are the Charge Transfer Descriptors Affected by the Quality of the Underpinning Electronic Density? *J. Comput. Chem.* **2018**, *39* (12), 735–742. https://doi.org/10.1002/jcc.25144.

(46) Rohatgi, A. Webplotdigitizer: Version 4.4. *https://automeris.io/WebPlotDigitizer*. 2020.

(47) Jorgensen, W. L.; Chandrasekhar, J.; Madura, J. D.; Impey, R. W.; Klein, M. L. Comparison of Simple Potential Functions for Simulating Liquid Water Liquid Water. *J. Chem. Phys.* **1998**, *79*, 926–935.

(48) Grimme, S.; Ehrlich, S.; Goerigk, L. Effect of the Damping Function in Dispersion Corrected Density Functional Theory. *J. Comput. Chem.* **2011**, *32* (7), 1456–1465. https://doi.org/10.1002/jcc.

(49) Luehr, N.; Jin, A. G. B.; Martínez, T. J. Ab Initio Interactive Molecular Dynamics on Graphical Processing Units (GPUs). *J. Chem. Theory Comput.* **2015**, *11* (10), 4536–4544. https://doi.org/10.1021/acs.jctc.5b00419.

(50) Furche, F.; Ahlrichs, R. Adiabatic Time-Dependent Density Functional Methods for Excited State Properties. *J. Chem. Phys.* **2002**, *117*, 7433. https://doi.org/10.1063/1.1508368.

(51) Liu, F.; Gan, Z.; Shao, Y.; Hsu, C.; Dreuw, A.; Head-gordon, M.; Miller, B. T.; Brooks, B. R.; Yu, J.; Furlani, T. R. *et al.* A Parallel Implementation of the Analytic Nuclear Gradient for Time-Dependent Density Functional Theory within the Tamm – Dancoff Approximation. *Mol. Phys.* **2010**, *108*, 2791–2800. https://doi.org/10.1080/00268976.2010.526642.

(52) Eric, B.; Savarese, M.; Adamo, C.; Jacquemin, D. Accuracy of TD-DFT Geometries : A Fresh Look. *J. Chem. Theory Comput.* **2018**, *14*, 3715–3727. https://doi.org/10.1021/acs.jctc.8b00311.

(53) Bousquet, D.; Fukuda, R.; Maitarad, P.; Jacquemin, D.; Cio, I.; Adamo, C.; Ehara, M. Excited-State Geometries of Heteroaromatic Compounds : A Comparative TD-DFT and SAC -CI Study. *J. Chem. Theory Comput.* **2013**, *9*, 2368–2379.

(54) Guido, C. A.; Jacquemin, D.; Adamo, C.; Mennucci, B. On the TD-DFT Accuracy in Determining Single and Double Bonds in Excited-State Structures of Organic

Molecules. *J. Phys. Chem. A* **2010**, *114*, 13402–13410.

(55) Wang, J.; Durbeej, B. How Accurate Are TD-DFT Excited-State Geometries Compared to DFT Ground-State Geometries? *J. Comput. Chem.* **2020**, 1718–1729. https://doi.org/10.1002/jcc.26213.

(56) Tuna, D.; Lu, Y.; Koslowski, A.; Thiel, W. Semiempirical Quantum-Chemical Orthogonalization-Corrected Methods : Benchmarks of Electronically Excited States. *J. Chem. Theory Comput.* **2016**, *12*, 4400–4422. https://doi.org/10.1021/acs.jctc.6b00403.

(57) Duan, H. D.; Mohamed-Raseek, N.; Miller, A. F. Spectroscopic Evidence for Direct Flavin-Flavin Contact in a Bifurcating Electron Transfer Flavoprotein. *J. Biol. Chem.* **2020**, *295* (36), 12618–12634. https://doi.org/10.1074/jbc.RA120.013174.

(58) Schreiber, M.; Silva-Junior, M. R.; Sauer, S. P. A.; Thiel, W. Benchmarks for Electronically Excited States: CASPT2, CC2, CCSD, and CC3. *J. Chem. Phys.* **2008**, *128* (13). https://doi.org/10.1063/1.2889385.

(59) Harbach, P. H. P.; Wormit, M.; Dreuw, A. The Third-Order Algebraic Diagrammatic Construction Method (ADC(3)) for the Polarization Propagator for Closed-Shell Molecules: Efficient Implementation and Benchmarking. *J. Chem. Phys.* **2014**, *141* (6). https://doi.org/10.1063/1.4892418.

(60) Kar, R. K.; Borin, V. A.; Ding, Y.; Matysik, J.; Schapiro, I. Spectroscopic Properties of Lumiflavin: A Quantum Chemical Study. *Photochem. Photobiol.* **2019**, *95* (2), 662–674. https://doi.org/10.1111/php.13023.

(61) Salzmann, S.; Marian, C. M. Effects of Protonation and Deprotonation on the Excitation Energies of Lumiflavin. *Chem. Phys. Lett.* **2008**, *463*, 400–404. https://doi.org/10.1016/j.cplett.2008.08.050.

(62) Hasegawa, J. ya; Bureekaew, S.; Nakatsuji, H. SAC-CI Theoretical Study on the Excited States of Lumiflavin: Structure, Excitation Spectrum, and Solvation Effect. *J. Photochem. Photobiol. A Chem.* **2007**, *189* (2–3), 205–210. https://doi.org/10.1016/j.jphotochem.2007.01.033.

(63) Neiss, C.; Saalfrank, P.; Parac, M.; Grimme, S. Quantum Chemical Calculation of Excited States of Flavin-Related Molecules. *J. Phys. Chem. A* **2003**, *107* (1), 140–147. https://doi.org/10.1021/jp021671h.

(64) Choe, Y.-K.; Nagase, S.; Nishimoto, K. Theoretical Study of the Electronic Spectra of Oxidized and Reduced States of Lumiflavin and Its Derivative. *J. Comput. Chem.* **2007**, *28*, 727–739. https://doi.org/10.1002/jcc.20533.

(65) Salzmann, S.; Tatchen, J.; Marian, C. M. The Photophysics of Flavins: What Makes the Difference between Gas Phase and Aqueous Solution? *J. Photochem. Photobiol. A Chem.* **2008**, *198* (2–3), 221–231. https://doi.org/10.1016/j.jphotochem.2008.03.015.

(66) Walsh, J. D.; Miller, A.-F. NMR Shieldings and Electron Correlation Reveal Remarkable Behavior on the Part of the Part of the Flavin N5 Reactive Center. *J. Phys. Chem. B* **2003**, *107* (3), 854–863. https://doi.org/10.1021/jp022005j.

(67) Conrad, K. S.; Manahan, C. C.; Crane, B. R. Photochemistry of Flavoprotein Light Sensors. *Nat. Chem. Biol.* **2014**, *10* (10), 801–809. https://doi.org/10.1038/nchembio.1633.

(68) Hou, S.; Bernath, P. F. Relationship between Dipole Moments and Harmonic Vibrational Frequencies in Diatomic Molecules. *J. Phys. Chem. A* **2015**, *119*, 1435–1438. https://doi.org/10.1021/acs.jpca.5b00993.

(69) Hansch, C.; Leo, A.; Taft, R. W. A Survey of Hammett Substituent Constants and Resonance and Field Parameters. *Chem. Rev.* **1991**, *91* (2), 165–195. https://doi.org/10.1021/cr00002a004.

(70) Lewis, M.; Bagwill, C.; Hardebeck, L. K. E.; Wireduaah, S. The Use of Hammett Constants to Understand the Non-Covalent Binding of Aromatics. *Comput. Struct. Biotechnol. J.* **2012**, *1* (1), e201204004. https://doi.org/10.5936/csbj.201204004.

(71) Etz, B. D.; Duclos, J. M.; Vyas, S. Investigating the Photochemistry of C7 and C8 Functionalized N(5)-Ethyl-Flavinium Cation: A Computational Study. *J. Phys. Chem. A* **2020**, *124* (21), 4193–4201. https://doi.org/10.1021/acs.jpca.0c01938.

(72) Vdovin, A.; Slenczka, A.; Dick, B. Electronic Spectroscopy of Lumiflavin in Superfluid Helium Nanodroplets. *Chem. Phys.* **2013**, *422*, 195–203. https://doi.org/10.1016/j.chemphys.2012.11.001.

(73) Zheng, Y. J.; Ornstein, R. L. A Theoretical Study of the Structures of Flavin in Different Oxidation and Protonation States. *J. Am. Chem. Soc.* **1996**, *118* (39), 9402–9408. https://doi.org/10.1021/ja9608151.

(74) Udvarhelyi, A.; Olivucci, M.; Domratcheva, T. Role of the Molecular Environment in Flavoprotein Color and Redox Tuning: QM

Cluster versus QM/MM Modeling. *J. Chem. Theory Comput.* **2015**, *11* (8), 3878–3894. https://doi.org/10.1021/acs.jctc.5b00197.

(75) Harrison, J. F. On the Role of the Electron Density Difference in the Interpretation of Molecular Properties. *J. Chem. Phys.* **2003**, *119*, 19–21. https://doi.org/10.1063/1.1610432.

(76) Plasser, F. Visualisation of Electronic Excited-State Correlation in Real Space. *ChemPhotoChem* **2019**, *3*, 702–706. https://doi.org/10.1002/cptc.201900014.

(77) Karasulu, B.; Götze, J. P.; Thiel, W. Assessment of Franck-Condon Methods for Computing Vibrationally Broadened UV-Vis Absorption Spectra of Flavin Derivatives: Riboflavin, Roseoflavin, and 5-Thioflavin. *J. Chem. Theory Comput.* **2014**, *10* (12), 5549–5566. https://doi.org/10.1021/ct500830a.

(78) Knippenberg, S.; Gieseking, R. L.; Rehn, D. R.; Mukhopadhyay, S.; Dreuw, A.; Brédas, J. L. Benchmarking Post-Hartree-Fock Methods to Describe the Nonlinear Optical Properties of Polymethines: An Investigation of the Accuracy of Algebraic Diagrammatic Construction (ADC) Approaches. *J. Chem. Theory Comput.* **2016**, *12* (11), 5465–5476. https://doi.org/10.1021/acs.jctc.6b00615.

(79) Schwinn, K.; Ferré, N.; Huix-Rotllant, M. UV-Visible Absorption Spectrum of FAD and Its Reduced Forms Embedded in Cryptochrome Protein. *Phys. Chem. Chem. Phys.* **2020**, *22*, 12447–12455. https://doi.org/10.1039/D0CP01714K.

(80) Choi, C. H.; Kertesz, M.; Karpfen, A. The Effects of Electron Correlation on the Degree of Bond Alternation and Electronic Structure of Oligomers of Polyacetylene. *J. Chem. Phys.* **1997**, *107* (17), 6712–6721. https://doi.org/10.1063/1.474914.

(81) Jacquemin, D.; Perpète, E. A.; Ciofini, I.; Adamo, C. Assessment of Recently Developed Density Functional Approaches for the Evaluation of the Bond Length Alternation in Polyacetylene. *Chem. Phys. Lett.* **2005**, *405* (4–6), 376–381. https://doi.org/10.1016/j.cplett.2005.02.037.

(82) Jacquemin, D.; Femenias, A.; Chermette, H.; Ciofini, I.; Adamo, C.; André, J. M.; Perpète, E. A. Assessment of Several Hybrid DFT Functionals for the Evaluation of Bond Length Alternation of Increasingly Long Oligomers. *J. Phys. Chem. A* **2006**, *110* (17), 5952–5959. https://doi.org/10.1021/jp060541w.

(83) Lee, M.; Hong, J.; Seo, D. H.; Nam, D. H.; Nam, K. T.; Kang, K.; Park, C. B. Redox Cofactor from Biological Energy Transduction as Molecularly Tunable Energy-Storage Compound. *Angew. Chemie - Int. Ed.* **2013**, *52* (32), 8322–8328. https://doi.org/10.1002/anie.201301850.

(84) Schopfer, L. M.; Wessiak, A.; Massey, V. Interpretation of the Spectra Observed during Oxidation of P-Hydroxybenzoate Hydroxylase Reconstituted with Modified Flavins. *J. Biol. Chem.* **1991**, *266* (20), 13080–13085. https://doi.org/10.1016/s0021-9258(18)98806-x.

(85) Sarma, R.; Sloan, M. J.; Miller, A. F. Flavin-Sensitized Electrode System for Oxygen Evolution Using Photo-Electrocatalysis. *Chem. Commun.* **2016**, *52* (57), 8834–8837. https://doi.org/10.1039/c6cc01479h.

(86) Orita, A.; Verde, M. G.; Sakai, M.; Meng, Y. S. A Biomimetic Redox Flow Battery Based on Flavin Mononucleotide. *Nat. Commun.* **2016**, *7*, 1–8. https://doi.org/10.1038/ncomms13230.

(87) Yu, X.; Eymur, S.; Singh, V.; Yang, B.; Tonga, M.; Bheemaraju, A.; Cooke, G.; Subramani, C.; Venkataraman, D.; Stanley, R. J. *et al.* Flavin as a Photo-Active Acceptor for Efficient Energy and Charge Transfer in a Model Donor-Acceptor System. *Phys. Chem. Chem. Phys.* **2012**, *14* (19), 6749–6754. https://doi.org/10.1039/c2cp40073a.

(88) Reckmeier, C. J.; Wang, Y.; Zboril, R.; Rogach, A. L. Influence of Doping and Temperature on Solvatochromic Shifts in Optical Spectra of Carbon Dots. *J. Phys. Chem. C* **2016**, *120* (19), 10591–10604. https://doi.org/10.1021/acs.jpcc.5b12294.

(89) Beztsinna, N.; Solé, M.; Taib, N.; Bestel, I. Bioengineered Riboflavin in Nanotechnology. *Biomaterials* **2016**, *80*, 121–133. https://doi.org/10.1016/j.biomaterials.2015.11.050.

(90) Richtar, J.; Heinrichova, P.; Apaydin, D. H.; Schmiedova, V.; Yumusak, C.; Kovalenko, A.; Weiter, M.; Sariciftci, N. S.; Krajcovic, J. Novel Riboflavin-Inspired Conjugated Bio-Organic Semiconductors. *Molecules* **2018**, *23* (9), 1–18. https://doi.org/10.3390/molecules23092271.

(91) Mohammed, N.; Wiles, A. A.; Belsley, M.; Fernandes, S. S. M.; Cariello, M.; Rotello, V. M.; Raposo, M. M. M.; Cooke, G. Synthesis and Characterisation of Push-Pull Flavin Dyes with Efficient Second Harmonic Generation (SHG) Properties. *RSC Adv.* **2017**, *7* (39), 24462–24469. https://doi.org/10.1039/c7ra03400h.

(92) Kodali, G.; Siddiqui, S. U.; Stanley, R. J. Charge Redistribution in Oxidized and Semiquinone E. Coli DNA Photolyase upon

Photoexcitation: Stark Spectroscopy Reveals a Rationale for the Position of Trp382. *J. Am. Chem. Soc.* **2009**, *131* (13), 4795–4807. https://doi.org/10.1021/ja809214r.

(93) Lin, L.; Xie, K.; Beaucamp, M.; Job, N.; Penhoat, M. Riboflavin as a Bioorganic Solar Fuel: Photoredox Chemistry Rationalized and Accelerated in a Miniaturized Flow Photoreactor. *ChemPhotoChem* **2019**, *3* (4), 198–203. https://doi.org/10.1002/cptc.201800236.

(94) Ilic, S.; Brown, E. S.; Xie, Y.; Maldonado, S.; Glusac, K. D. Sensitization of P-GaP with Monocationic Dyes: The Effect of Dye Excited-State Lifetime on Hole Injection Efficiencies. *J. Phys. Chem. C* **2016**, *120* (6), 3145–3155. https://doi.org/10.1021/acs.jpcc.5b10474.

(95) Yorita, K.; Misaki, H.; Palfey, B. A.; Massey, V. On the Interpretation of Quantitative Structure–Function Activity Relationship Data for Lactate Oxidase. *Proc. Natl. Acad. Sci. USA* **2000**, *97* (6), 2480–2485.

(96) Ortiz-maldonado, M.; Ballou, D. P.; Massey, V. A Rate-Limiting Conformational Change of the Flavin in p-Hydroxybenzoate Hydroxylase Is Necessary for Ligand Exchange and Catalysis: Studies with 8-Mercapto- and 8-Hydroxy-Flavins. *Biochemistry* **2001**, *40*, 1091–1101.

(97) Sikorski, M.; Sikorska, E.; Koziolowa, A.; Moreno, R. G.; Bourdelande, J. L.; Steer, R. P.; Wilkinson, F. Photophysical Properties of Lumichromes in Water. *J. Photochem. Photobiol. B Biol.* **2001**, *60*, 114–119.

(98) Moore, E. .; Cardemil, E.; Massey, V. Production of a Covalent Flavin Linkage in Lipoamide Dehydrogenase. *J. Biol. Chem.* **1978**, *253* (18), 6413–6422. https://doi.org/10.1016/S0021-9258(19)46948-2.

(99) Ghisla, S.; Massey, V. New Flavins for Old: Artificial Flavins as Active Site Probes of Flavoproteins. *J. Biochem.* **1986**, *239*, 1–12.

(100) Murthy, Y. V. S. N.; Massey, V. Synthesis and Properties of 8-CN-Flavin Nucleotide Analogs and Studies with Flavoproteins. *J. Biol. Chem.* **1998**, *273* (15), 8975–8982. https://doi.org/10.1074/jbc.273.15.8975.

(101) Robbins, J. M.; Souffrant, M. G.; Hamelberg, D.; Gadda, G.; Bommarius, A. S. Enzyme-Mediated Conversion of Flavin Adenine Dinucleotide (FAD) to 8-Formyl FAD in Formate Oxidase Results in a Modified Cofactor with Enhanced Catalytic Properties. *Biochemistry* **2017**, *56*, 3800–3807. https://doi.org/10.1021/acs.biochem.7b00335.

(102) Tyagi, A.; Zirak, P.; Penzkofer, A.; Mathes, T.; Hegemann, P.; Mack, M.; Ghisla, S. Absorption and Emission Spectroscopic Characterisation of 8-Amino-Riboflavin. *Chem. Phys.* **2009**, *364* (1–3), 19–30. https://doi.org/10.1016/j.chemphys.2009.08.005.

(103) Moore, E. G.; Ghisla, S.; Massey, V. Properties of Flavins Residues Where the 8-Methyl Group Is Replaced by Mercapto- Residues. *J. Biol. Chem.* **1979**, *254* (17), 8173–8178. https://doi.org/10.1016/S0021-9258(19)86872-2.

(104) Massey, V.; Ghisla, S.; Moore, E. G. 8-Mercaptoflavins as Active Site Probes of Flavoenzymes. *J. Biol. Chem.* **1979**, *254* (19), 9640–9650. https://doi.org/10.1016/S0021-9258(19)83564-0.

(105) Ghisla, S.; Mayhew, S. G. Identification and Properties of 8-Hydroxyflavin-Adenine Dinucleotide in Electron-Transferring Flavoprotein from Peptostreptococcus Elsdenii. *Eur. J. Biochem.* **1976**, *190*, 373–390.